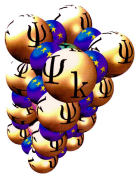

Ψ_k Scientific Highlight Of The Month

No. 126 **February 2015**

Cisplatin resistance in anticancer therapy: insights by hybrid Car-Parrinello/molecular mechanics simulations

Vania Calandrini[1,*], Giulia Rossetti[1,2], Trung Hai Nguyen[1], and Paolo Carloni[1]

[1]Computational Biomedecine section (INM-9), Institute for Neuroscience and Medecine (INM), and (IAS-5), Institute of Advanced Simulation (IAS), 52425 Jülich, Germany

[2]Jülich Supercomputing Center (JSC), Jülich, Germany

[*]v.calandrini@grs-sim.de

Cisplatin resistance in anticancer therapy: insights by hybrid Car-Parrinello/molecular mechanics simulations

Vania Calandrini[1], Giulia Rossetti[1,2], Trung Hai Nguyen[1] and Paolo Carloni[1]

[1]Computational Biomedicine section (INM-9), Institute for Neuroscience and Medicine (INM), and (IAS-5), Institute of Advanced Simulation (IAS), 52425 Jülich, Germany
[2]Jülich Supercomputing Center (JSC), Jülich, Germany

Abstract
The drug cis-diamminedichloroplatinum(II) (cisplatin) has revolutionized anticancer therapy back in the late seventies. It triggers tumor-cell death by binding to DNA. Cisplatin treats very successfully testicular and ovarian tumors, along with a variety of other cancers. Unfortunately, cisplatin-based therapies are plagued by resistance mechanisms that cause very severe side effects. Characterizing the interactions of cisplatin with its cellular partners is of great importance to design new platinum-based anticancer drugs able to overcome cisplatin's resistance issues. First principle studies have revealed themselves as powerful tools for predictions of structural determinants and of the energetics of these systems. Here will we review our recent work on hybrid Car-Parrinello Molecular Dynamics/Molecular Mechanics (CPMD/MM) simulations along with molecular spectroscopy calculations. The calculations uncover details of the molecular recognition process between platinated DNA and a key cellular partner and provide an unprecedented view on the structural features of platinated proteins involved in drug resistance.

1. Introduction

Cisplatin (cis-diamminedichloridoplatinum(II)) is one of the most widely used drugs in anticancer chemotherapy.[1-6] Its beneficial effect is mainly caused by the formation of adducts with DNA. This causes DNA lesions, which in turn lead to tumor cell apoptosis.[7, 8] However cisplatin's therapeutic efficacy is strongly limited by the appearance of resistance mechanisms after repeated administrations of the drug.[1, 3, 4] These stem from interactions of the drug with unwanted cellular partners before its binding to DNA (*pre-target resistance*), from alterations of DNA-cisplatin adducts (*on-target resistance*); from cellular responses to cisplatin-mediated DNA damage (*post-target resistance*); from alteration of other cellular

pathways not directly linked with cisplatin-elicited signals (*off-target resistance*)[9].
Understanding the molecular basis of cisplatin resistance is of paramount importance for designing new Pt-based compounds able to circumvent drug resistance. [4, 10] A key step in accomplishing this goal is to characterize structurally and energetically the adducts of cisplatin with the cellular partners involved in drug resistance. Experimentally, this characterization is partially lacking. Our group for the last year has then addressed the problem using molecular simulations approaches.
In the platinated adducts, the stereochemistry of the transition metal coordination polyhedron is dictated by quantum mechanical effects. Hence, this problem is amenable for quantum mechanical/molecular mechanical (QM/MM) simulation, in which the platinated region (where the electronic degrees of freedom are relevant) is described by a quantum mechanical electronic structure method. Here we use Density Functional Theory (DFT)-based hybrid Car and Parrinello molecular dynamics/Molecular Mechanics (CPMD/MM) simulations[11 12 13]. The CPMD/MM scheme describes the relevant electronic degrees of freedom along with extended environmental effects. DFT is very successful because of its accuracy/computational-cost ratio for transition metal complexes.[14-17] The QM region is mechanically and electrostatically coupled with the rest of the system, which is treated using empirical biomolecular force fields like, AMBER,[18] GROMOS[19] or CHARMM.[20(i)] In our applications here, the MM part is described by AMBER force field using routines from Gromos96 code.[19(ii)] The comparison between experimental and theoretical spectroscopy (CD, EXAFS, and ^{1}H, ^{13}C, ^{15}N, and ^{195}Pt NMR chemical shifts), as well as thermodynamic data, have established the accuracy of the structural predictions. [25-28]

2. Cisplatin resistance

In the following we will review some recent application of CPMD/MM MD simulations to both structural predictions and free energy calculations in proteins and in protein complexes involved in pre-target and on-target cisplatin resistance.

2. 1 Pre-target resistance

Cancer cells elude the cytotoxic potential of cisplatin before binding to DNA by a reduced intra- cellular accumulation of cisplatin and by an increased sequestration/efflux of cisplatin cytoplasmic 'scavengers' proteins with nucleophilic properties [9].
Several proteins involved in the copper homeostasis, and able to bind cisplatin, play a major role for regulating the cellular accumulation of the drug. [4, 29-33] The high-affinity copper transporter Ctr1 drives cisplatin uptake via active transport.[34] The ATPase copper pumps ATP7A/ATP7B have been found to be responsible for sequestration and efflux of cisplatin.[35, 36] Atox1 proteins has been suggested to be involved in platinum delivery to the ATPases[37, 38] and also in the influx of cisplatin, by controlling the cisplatin-induced down regulation of

[i] The reader may refer to a recent review for an extensive discussion of the method and of its practical implementation[21].
[ii] Hybrid simulations are computationally costly and may cover currently a timescale of a ns or less.[21, 22] To circumvent this problem, in some of the applications, we have applied the force matching procedure of refs. [23, 24] to the CPMD/MM simulations, in order to derive AMBER-type force field parameters for the Pt moieties. [25, 26] This allow to run longer classical MD simulations based on the new force field parameters.

Ctr1 through ubiquitination.[29, 39] Furthermore, Atox1 has been found to translocate to the nucleus in the response to copper exposure[40] . This raises the question of whether it could also be involved in the delivery of cisplatin to DNA.

Experimental investigations had provided *qualitative* information on these platinated proteins in solution. Specifically, the met-rich N-terminal extracellular domain of ***Ctr1***, which is know to bind copper ions, had been identified as a putative cisplatin binding site.[41-43] Met sulfur is indeed a good donor atom for platinum.[44] NMR and Electrospray Mass spectrometry[43] on the model peptide MTGMKGMS (Mets7), mimicking one of the Met-rich motifs of the N-terminal extracellular domain of yeast Ctr1*,* suggested that (i) Cisplatin loses all of its ligands upon reaction with Mets7 and the metal ion binds to the three Met residues and completes its coordination shell with a fourth ligand that can be a chloride or a water/hydroxyl oxygen. (ii) Transplatin (the inactive form of cisplatin) loses only the chlorido ligands, which are replaced by Met residues.

The **ATP7A/ATP7B** copper pumps share homologous structures made of 8 transmembrane domains and 6 soluble domains at the N-terminal cytosolic side containing six metal-binding domains (MBDs)[45, 46] with the same CxxC motif (C = cysteine, x = aminoacid other than C). Binding of cisplatin to the CxxC motif of the copper transporter ATP7B had been reported by several authors.[37, 38, 47-50] In particular, EXAFS studies on platinum-bound second MBD of ATP7B showed that Pt is cis-coordinated to the thiolate groups of the two cysteines[37] (the other two ligands were phosphorus atoms of tris(2-carboxyethyl)phosphine (TCEP) used as reducing agent). ^{1}H, ^{13}C and ^{1}H, ^{15N} HSQC spectroscopy data along with Electrospray Mass Spectrometry (ESI-MS) data on the first cytosolic domain of ATP7A[51] (79 aminoacids, Mnk1 hereafter) showed that in solution, under anaerobic conditions and in the absence of a reducing agent, the nearly exclusive adduct formed upon the interaction between cisplatin and Mnk1 is a monomer in which the Pt ion binds to Cys19 and Cys22 sulphur atoms while retaining the two cis ammine ligands.

Electrospray Ionization Mass Spectrometry (ESI-MS) and NMR spectroscopy[52, 53] provided information on cisplatin binding mode to **Atox1** in water solution. Similarly to what happens in the reaction with the structurally similar Mnk1 protein, the $[Pt(NH_3)_2]^{2+}$ moiety binds to Cys12 and Cy15 residues of Atox1 keeping the two ammines and that the adduct is monomeric[52, 53]. Note that this binding mode is different from the one evidenced in crystallographic structures,[54] where 1:1 and 1:2 complexes between human Atox1 and cisplatin were observed with different coordination to that in solution.[25]

Hybrid CPMD/MM simulations were used to investigate the apo-proteins (I in Figures 1,2, and 3) and *in silico* model adducts based on the qualitative binding modes of metal ion inferred from experiments (C_i and T_i in Figure1, and II in Figures 2 and 3, see section 3.1 for computational details). Spectroscopic data were thus calculated as averages over the configurations explored along the CPMD/MM trajectories and compared to the available experimental counterparts (CD, EXAFS, and ^{1}H, ^{13}C, ^{15}N, and ^{195}Pt NMR chemical shifts) in order to validate or disprove the models (see section 3.2 for computational details). To test the capability of our computational approach to unambiguously discriminate the correct coordination and folding from incorrect ones, the same calculations were performed on three alternative binding models of the first cytosolic domain of ATP7A, different from that inferred from experiments, yet still plausible from a chemical point of view (A-C in Figure. 2).

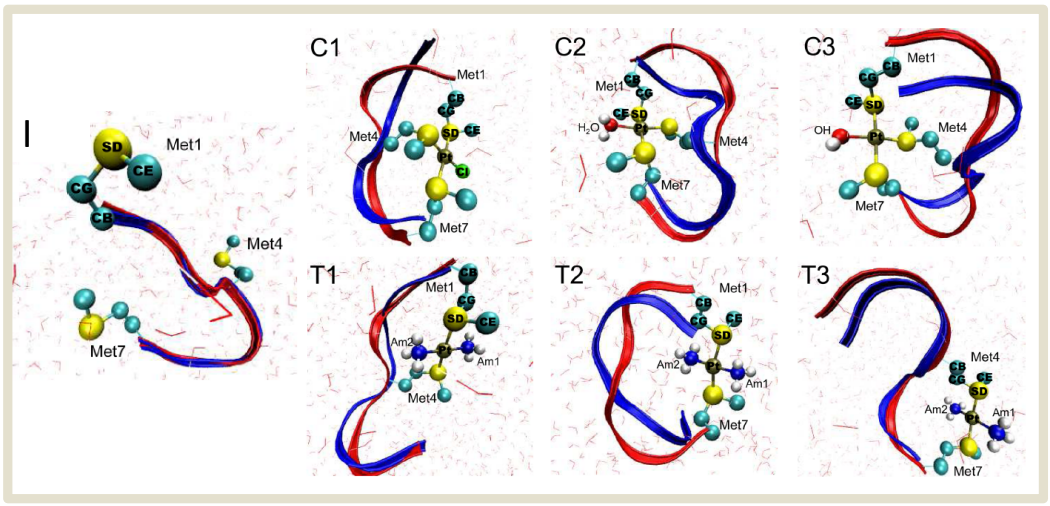

c

Table1: Cisplatin/Mets7

system	chemical shifts
experiment	-4100
C1	-3815 (321)
C2	-2793 (361)
C3	-3571 (382)

Table2: Transplatin/Mets7

system	chemical shifts
experiment	-2900
T1	-2793 (353)
T2	-3121 (347)
T3	-2751 (286)

Figure 1. **Panel (a)**: Readapted from ref.[25]. Structural models of platinated (C_i and T_i) and Apo (I) peptides emerging from replica exchange with solute tempering (REST) [55] classical MD simulations and CPMD/MM simulations. The backbone conformations of the last CPMD/MM snapshot (in red ribbons) and a representative REST snapshot (in blue ribbons) are superimposed. The QM atoms are shown in stick-and-balls (CB ≡ C_β, CG ≡ C**γ**, CE ≡ C**ε**). Water is shown in lines. Counterions are not shown for the sake of clarity. **Panel (b)**: Reprinted with permission from ref.[25] Copyright 2012 American Chemical Society. Calculated and experimentally measured CD spectra of cisplatin/Mets7 (left) and transplatin/Mets7 (right) adducts. **Panel (c):** [195] Pt NMR Chemical Shifts (in ppm) of the Cisplatin/Mets7 (C1– C3) and Transplatin/Mets7 (T1– T3) Adducts.

For **Mets7,** the comparison between experimental and calculated CD spectra (Figure1) shows that the C3 model in which the ligands of the Pt(II) ion are three Met residues and a hydroxyl group (Figure 1), gives the most important contribution to the total CD. C2 (Figure1) is also compatible with the measured CD while C1 model (Figure 1) shows much worse correspondence. In the case of the transplatin/Mets7 CD spectrum, the T1 model (coordination to platinum of Met1 and Met4, Figure 1) is likely to give a much greater contribution to the total CD than those of the other two models.

The comparison between calculated and experimental EXAFS spectra of the three C models indicates that model C1 (chlorido species), which did not contribute appreciably to the CD spectra, give instead a significant contribution to the EXAFS spectra (see ref. [25] for more details). This is compatible with the fact that, differently from the CD spectra, the EXAFS spectra were taken at considerably higher chloride concentration.

The calculated ^{1}H and ^{13}C NMR chemical shifts are in rather good agreement with the experimental chemical shifts and indicate that platinum binding causes a downfield shift of the NMR signals belonging to the Met residues bounded to the platinum, which is compatible with the experiment (see ref. [25] for more details). The calculations also confirm a contribution of models T2 and T3 to the overall spectra to account for the downfield shift observed for γ-CH_2 and ε-CH_3 of all methionines of Mets7 (see ref. [25] for more details). The

calculated ^{195}Pt chemical shifts (Figure1) also show that model C1 can give a relevant contribution to the experimental spectrum taken at a rather high chloride concentration. In contrast, model C2, the computed spectrum of which significantly deviates from the experimental one, contributes much less.

The self-consistency of the CPMD/MM structures is further supported by their compatibility with the local structures obtained from replica exchange with solute tempering [55] classical MD simulations based on the force field parameters of the Pt-moieties derived via force-matching approach. [23, 24] The new force field parameters have been estimated by averaging over 300 snapshots sampled along the CPMD/MM trajectories (See section 3.3 for computational details).

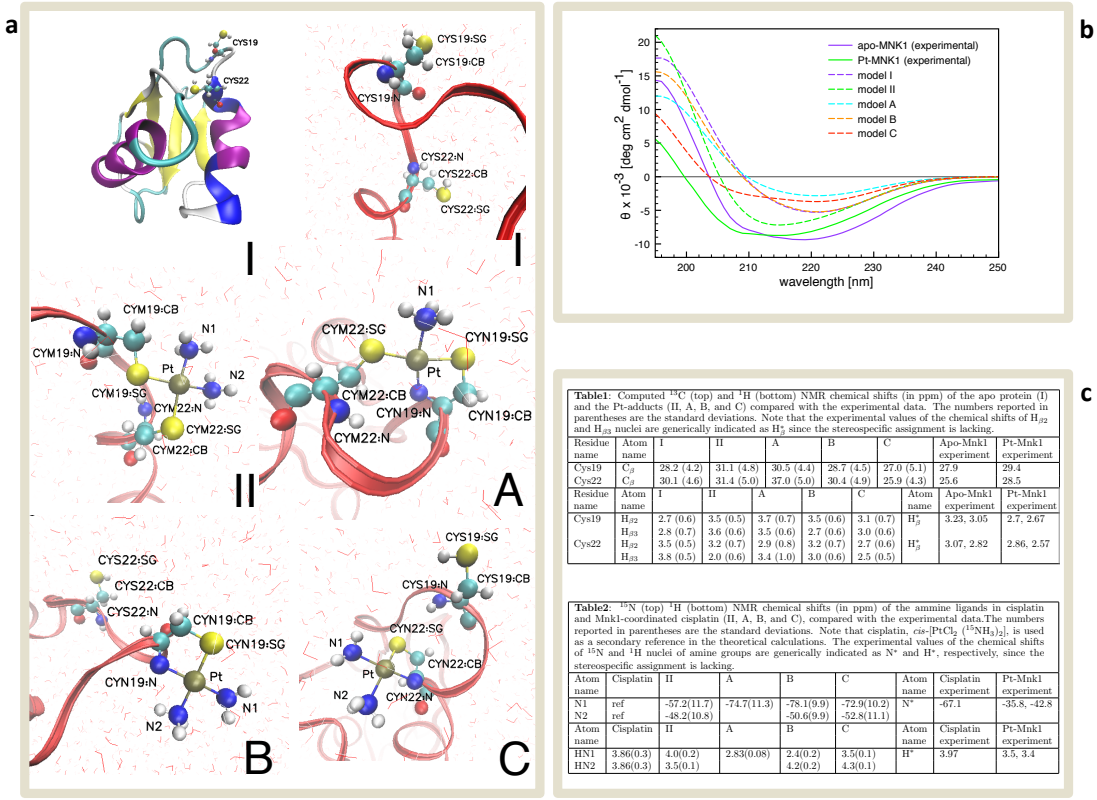

Table1: Computed ^{13}C (top) and ^{1}H (bottom) NMR chemical shifts (in ppm) of the apo protein (I) and the Pt-adducts (II, A, B, and C) compared with the experimental data. The numbers reported in parentheses are the standard deviations. Note that the experimental values of the chemical shifts of $H_{\beta 2}$ and $H_{\beta 3}$ nuclei are generically indicated as H^*_β since the stereospecific assignment is lacking.

Residue name	Atom name	I	II	A	B	C	Apo-Mnk1 experiment	Pt-Mnk1 experiment
Cys19	C_β	28.2 (4.2)	31.1 (4.8)	30.5 (4.4)	28.7 (4.5)	27.0 (5.1)	27.9	29.4
Cys22	C_β	30.1 (4.6)	31.4 (5.0)	37.0 (5.0)	30.4 (4.9)	25.9 (4.3)	25.6	28.5

Residue name	Atom name	I	II	A	B	C	Atom name	Apo-Mnk1 experiment	Pt-Mnk1 experiment
Cys19	$H_{\beta 2}$	2.7 (0.6)	3.5 (0.5)	3.7 (0.7)	3.5 (0.6)	3.1 (0.7)	H^*_β	3.23, 3.05	2.7, 2.67
	$H_{\beta 3}$	2.8 (0.7)	3.6 (0.6)	3.5 (0.6)	2.7 (0.6)	3.0 (0.6)			
Cys22	$H_{\beta 2}$	3.5 (0.5)	3.2 (0.7)	2.9 (0.8)	3.2 (0.7)	2.7 (0.6)	H^*_β	3.07, 2.82	2.86, 2.57
	$H_{\beta 3}$	3.8 (0.5)	2.0 (0.6)	3.4 (1.0)	3.0 (0.6)	2.5 (0.5)			

Table2: ^{15}N (top) ^{1}H (bottom) NMR chemical shifts (in ppm) of the ammine ligands in cisplatin and Mnk1-coordinated cisplatin (II, A, B, and C), compared with the experimental data.The numbers reported in parentheses are the standard deviations. Note that cisplatin, *cis*-$[PtCl_2\ (^{15}NH_3)_2]$, is used as a secondary reference in the theoretical calculations. The experimental values of the chemical shifts of ^{15}N and ^{1}H nuclei of amine groups are generically indicated as N^* and H^*, respectively, since the stereospecific assignment is lacking.

Atom name	Cisplatin	II	A	B	C	Atom name	Cisplatin experiment	Pt-Mnk1 experiment
N1	ref	-57.2(11.7)	-74.7(11.3)	-78.1(9.9)	-72.9(10.2)	N^*	-67.1	-35.8, -42.8
N2	ref	-48.2(10.8)		-50.6(9.9)	-52.8(11.1)			

Atom name	Cisplatin	II	A	B	C	Atom name	Cisplatin experiment	Pt-Mnk1 experiment
HN1	3.86(0.3)	4.0(0.2)	2.83(0.08)	2.4(0.2)	3.5(0.1)	H^*	3.97	3.5, 3.4
HN2	3.86(0.3)	3.5(0.1)		4.2(0.2)	4.3(0.1)			

Figure 2. **Panel (a)**: From ref. [27]. Reproduced by permission of The Royal Society of Chemistry. Structural models of apo-Mnk1 (**I**) and platinated model adducts (**II**, **A**, **B**, and **C**) emerging from our CPMD/MM simulations based on the NMR structure of the apo protein. **II** is constructed based on the experimentally determined binding mode. **A–C** show other binding modes explored to test the robustness of the computational approach. Red ribbons represent the protein backbone; Cys19 and Cys22, along with the Pt-moiety, are shown in balls and sticks. Water molecules are represented by lines. Counterions, which neutralize the system, are not shown for sake of clarity. **Panel (b)**: Readapted from ref. [27]. Calculated and experimentally measured CD spectra of the apo protein and the Pt adducts. **Panel (c)**: ^{1}H, ^{13}C, (Table 1) and ^{1}H ^{15}N (Table 2) NMR chemical shifts (in ppm) of apo Mnk1 and its Pt-adduct.

As for **Mnk1** (first cytosolic domain of **ATP7A**), the calculated CD spectra of both apo protein (**I**) and the platinated adduct **II** (Figure2) qualitatively reproduce the main features of the experimental counterparts, namely the shift of the maximum negative ellipticity toward lower wavelengths upon platination, which indicates a loss of helical structure.

The calculated ^{1}H and ^{13}C chemical shifts of the apo protein (**I**) and model **II** (Figure2) are compatible with the experimental counterparts within the intrinsic errors of the methodology (7.6 ppm for ^{13}C chemical shift[56] and ~1 ppm for ^{1}H chemical shifts[13]).

Moreover, the calculations on model **II** reproduce the downfield shift observed experimentally for Cys19 and Cys22 $^{13}C_{\beta}$-chemical shifts upon platination.

The ^{15}N chemical shift is very sensitive to the nature of the donor atom in trans position, and therefore may be very diagnostic of the presence of sulphur coordination.[57, 58] Again model **II** proved to be compatible with the experimental data within the mean error intrinsic to the employed level of theory (Figure2). As far as the proton chemical shifts are concerned, all calculated values are essentially consistent with the experimental ones within the mean error intrinsic to the method (Figure2).[13]

These findings support the reliability of the structural models **I** and **II** in correctly reproducing both the apo protein and the platinated adduct. This is further confirmed by the comparison between the experimental data and models **A-C** (Figure2)**,** which represent binding modes qualitatively incompatible with the experiment. Several discrepancies, beyond the calculation errors, are noted for CD spectra, C_{β} chemical shifts and C_{β} downfield shift upon platination, which lead us to discard them by a progressive elimination procedure (see ref.[27] for more details). This finding establishes the accuracy of the model and supports the reliability of the 3D atomic structures derived from our simulations.

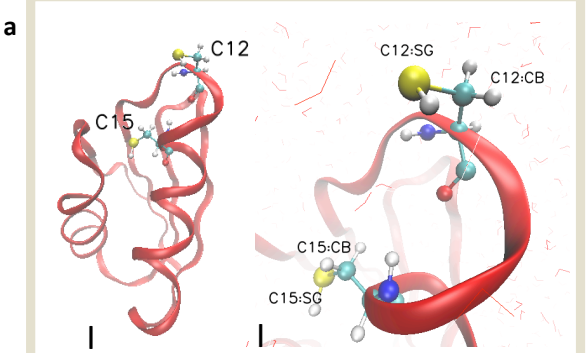

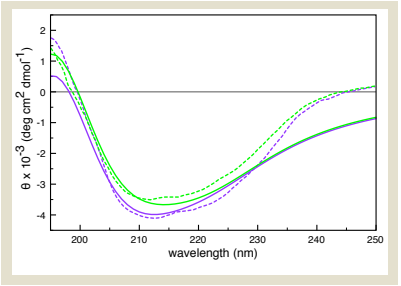

c

Table1: ^{13}C (top) ^{1}H (bottom) NMR chemical shifts (in ppm) of apo Atox1 (I) and its Pt-adduct (II) compared with the experimental data.[1]

Residue	Atom name	I	II		Apo Atox1 experiment	Pt-adduct experiment
Cys12	C_{β}	31.7 (3.9)	35.7 (4.0)		28.7	29.1
Cys15	C_{β}	29.4 (3.7)	35.9 (4.0)		27.1	28.9
Residue	Atom name	I	II	Atom name	Apo Atox1 experiment	Pt-adduct experiment
Cys12	$H_{\beta 2}$	3.9 (0.5)	3.8 (0.5)	H^{*}_{β}	3.31, 3.06	2.99, 2.66
	$H_{\beta 3}$	3.3 (0.5)	3.4 (0.6)			
Cys15	$H_{\beta 2}$	3.8 (0.6)	3.4 (0.5)	H^{*}_{β}	3.34, 2.87	2.88, 2.71
	$H_{\beta 3}$	2.6 (0.4)	3.4 (0.6)			

[1]The numbers reported in parentheses are the standard deviations. Note that the experimental values of the chemical shifts of $H_{\beta 2}$ and $H_{\beta 3}$ nuclei are generically indicated as H^{*}_{β} since the stereospecific assignment is lacking.

Table2: ^{15}N (top) ^{1}H (bottom) NMR chemical shifts (in ppm) of the amine ligands in cisplatin and in Atox1-cisplatin adduct (II) compared with the experimental data.[1]

Atom name	Cisplatin	II	Atom name	Cisplatin experiment	Pt-adduct experiment
N1	reference	-44.1 (7.8)	N^{*}	-67.1, -67.1	-42.5, -36.5
N2	reference	-52.1 (8.1)			
HN1	3.9 (0.3)	3.8 (0.1)	H^{*}	3.97, 3.97	3.43, 3.38
HN2	3.9 (0.3)	4.1 (0.2)			

[1]The numbers reported in parentheses are the standard deviations. Note that cisplatin (*cis*-$[PtCl_2(^{15}NH_3)_2]$) is used as a secondary reference in the theoretical calculations. The experimental values of the chemical shifts of ^{15}N and ^{1}H nuclei of amine groups are generically indicated as N^{*} and H^{*}, respectively, since the stereospecific assignment is lacking.

Figure 3: **Panel (a)**: Readapted from ref. [28]. Structural models of apo Atox1 (I) and its Pt-adduct (II) in aqueous solution as they emerge from CPMD/MM simulations (left: apo Atox1 backbone along with Cys12 and Cys15 side chains; right: close up on the Cys12/Cys15 region in apo Atox1; bottom: close up on the Cys12/Cys15 region in the Pt-adduct). The backbone of the protein is represented by a red ribbon. Cys12 and Cys15 residues, along with the Pt moiety, are represented in balls and sticks (color code: platinum in brown, sulfur in yellow, carbon in cyan, nitrogen in blue, and hydrogen in white). Water molecules are represented by lines (color code: oxygen in red and hydrogen in white). **Panel (b)**: Calculated (continuous lines) and experimental (dashed lines) CD spectra of apo Atox1 (violet) and the Pt-adduct (green). **Panel (c):** ^{1}H ^{13C} and ^{15}N NMR chemical shifts (in ppm) of apo Atox1 and the Pt-adduct compared with the experimental data.

For **Atox1**, the calculated CD spectra of both apo (I) and Pt-adduct (II) (Figure3) are in good

agreement with the experimental ones, which supports the reliability of our models in describing the global fold. The calculated ^{13}C chemical shifts (Figure3) of the β-methylene groups of Cys12 and Cys15 side chains reproduce the experimental data within one standard deviation, or, in the worst cases, within the typical error due to the employed level of theory for both apo- and Pt-Atox1 (7.6 ppm for ^{13}C chemical shift[56]). In addition, our calculations predict for the Cβ carbon of Cys12 and Cys15 a small downfield shift upon platination, which is compatible with the downfield shift observed experimentally. The calculated ^{15}N chemical shifts of the Pt-bound ammine ligands (Figure3) are compatible with the experimental data. They deviate from the experimental values by ~9 ppm, which is well below the typical error associated to this level of theory (13-16 ppm) [59]. These theoretical data thus correctly reproduce one of the most important experimental findings in favor of the presence of $^{15}NH_3$ groups trans to the S atoms of Cys 12 and Cys15. Also in the case of the chemical shifts of the ^{1}H (Figure 3), the calculated values are consistent with the experimental ones within one standard deviation or, in the worst cases, within the mean error intrinsic to the employed level of theory (~1 ppm for ^{1}H chemical shifts[13]). We therefore conclude that our 3D model, which is fully consistent with all of the spectroscopic data so far available, confidently represents the overall structure of the platinated Atox1 adduct in solution.

2.2 On-target resistance

Cisplatin exerts the cytotoxic activity by covalently binding DNA,[2, 6] forming preferentially (>80%) 1,2-intrastrand cross-links with guanines[2, 6, 8] that bend DNA. Nucleotide excision repair (NER) enzymes are able to remove the platinum lesions from DNA, leading to drug resistance.[2, 6, 8] Such a repair may be inhibited by chromosomal high-mobility group proteins (HMGB), HMGB1, HMGB2 and HMGB4 as shown by *in vitro*[60-62] and *in cell* experiments.[63] Notably, the binding affinity of the reduced state of HMGB1 protein for platinated DNA (Pt-DNA) is larger than that of the oxidized state, where two fully conserved cysteine residues (Cys22 and Cys44[64]) form an S-S bridge.[65] Both the reduced state and the Cys-Cys bridged protein could be present in disease conditions. This has lead to the hypothesis that the high activity of cisplatin towards testicular tumors could be due to the unique expression in the testis[64] of HMGB4, which lacks one of the two cysteines and hence cannot form the S-S bond.[65]

Hybrid CPMD/MM simulations were used to sample the configurational space of one of the HMGB proteins (HMGB1A) in complex with the platinated oligonucleotide $[Pt(NH_3)_2]^{2+}$-d(CCUCTCTG*G*ACCTTCC)-d(GGAGAGACCTGGAAGG)[66] (*G are platinated guanines) in both the reduced and oxidized state (S-S bridge between Cys22 and Cys44) of the protein[26] (see ref [26] and Figure 4). Specifically we treated at the quantum mechanical level the cisplatin moiety and the G8G9 bases while the rest was treated at the classical level (see section 3.1 for computational details). Using the force matching procedure of refs.[23, 24] over 200 snapshots sampled along the CPMD/MM trajectory, we derived AMBER-type force field parameters for the Pt moieties (section 3.3 for computational details). The latter were used to run well tempered Metadynamics[67-70] free energy calculations. This approach allowed the identification of the molecular basis of the recognition process as well as of the decreased affinity of oxidized HMGB1A for platinated DNA. The work by Lippard *et al*.[66] showed how the phenyl group of Phe37 in reduced HMGB1A inserts in between the cross-linked guanines

and the resulting stacking interaction contributes to the stabilization of the protein-DNA complex (Figure 4). Our computational investigation has shown that, indeed, this interaction locks the protein-DNA complex in the absolute free energy minimum (B in Figure 4) where, our calculated free energy is fairly consistent with the experimental data[65]. Moreover, the disruption of this interaction is the first step in the dissociation process, further supporting its key role in the stabilization of the complex.

Concerning oxidized HMGB1, the experimentally observed decrease in affinity upon protein oxidation and consequent formation of a Cys22-Cys44 disulfide bridge (5.5 kJ/mol)[65], has lead to the hypothesis that the high efficacy of cisplatin towards testicular tumors could be due to the exclusive presence in the testis of a member of the HMGB superfamily (the HMGB4 protein)[64, 65] that lacks one of the two cysteine residues. The latter protein cannot form the S-S bridge upon oxidation. Our calculations suggest that the decrease in binding free energy upon formation of the Cys22-Cys44 disulfide bridge is likely due to a structural rearrangement of helices H1 and H2, which causes Phe37, located on top of helix H2, to slightly withdraw from the hydrophobic notch formed by the cross-linked G8 and G9 bases (Figure 4). The latter result is rather remarkable since it shows that computational methods can correctly evaluate loss of stability consequent to small conformational changes.

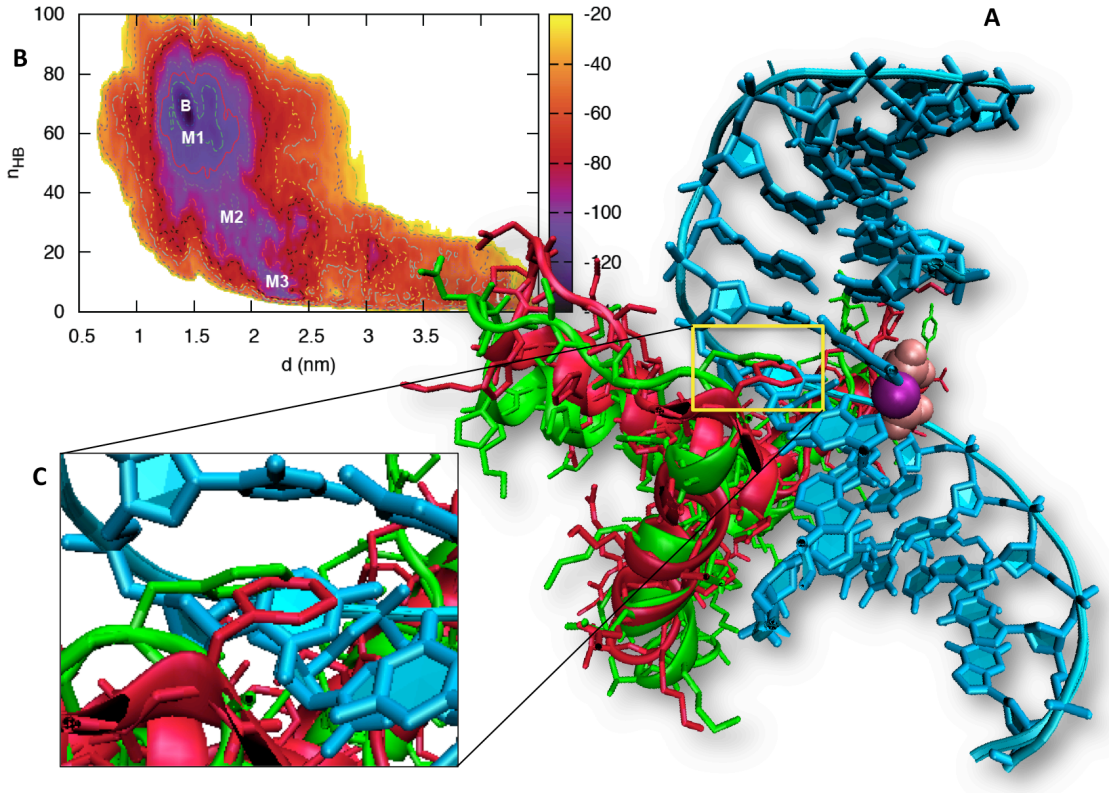

Figure 4. Reduced (green) and oxidized (red) HMGB1 in complex with platinated DNA (cyan) (**Panel A**) A close-up of Phe37 is offered (**Panel C**). The Free energy profile (**Panel B**) is projected on *d* and n_{HB} collective variables [*d* is the distance between the centers of mass of Pt-DNA and HMGB1A and n_{HB} is the number of hydrogen bonds at the interface between the two moieties]. B denotes the bound state while U represents the unbound minimum [Pt-DNA and HMGB1A protein ~4 nm apart]. M1-M5 are the local minima.

3. Computational Details

3.1 Hybrid CPMD/MM simulations

Hybrid CPMD/MM simulations were run with the BLYP recipe for the exchange−correlation functional. [71, 72] The QM part includes the platinum coordination polyhedron of each system along with the residues/bases of the binding site. The wave function was expanded in a plane-wave basis set up to an energy cutoff of 70 Ry for Mets7 and DNA and 90 Ry for Mnk1 and Atox1. Only the valence electrons were treated explicitly (in the case of Pt, electrons in the n = 5 shell were also included in the valence), while the core electrons were described using norm-conserving pseudopotentials of the Martins−Troullier type.[73] For Mets7 the QM atoms linked to the classical part by covalent bonds were saturated by "capping" hydrogen atoms, whilst for Mnk1 Atox1 and the DNA an adapted monovalent carbon pseudopotential was employed to saturate the dangling bonds in between the QM and MM regions.[74] Isolated system conditions were imposed in the QM part by employing the Martyna-Tuckerman scheme.[75] The MM part includes the rest of the system. The latter was described by the Amber99SB force field[76, 77] for the protein frame of Mets7, Atox1, and Mnk1, the Amber99SB-ILDN force field[76-78] for HMGB1A and DNA and the TIP3P[79] for water. Counterions were modeled using the Smith&Dang force field[80] for platinated Mets7 and Mnk1 systems and the Joung&Cheatham force field[81] for Pt-DNA*HMGB1A. The QM and MM parts were coupled using the fully Hamiltonian hierarchical approach.[68] Hybrid CPMD/MM simulations of the order of 10-20ps-long were carried out. For more details about CPMD/MM simulations refer to refs. [25-28].

3.2 Computational spectroscopy

CD and EXAFS spectra were calculated using respectively the web interface DichroCalc developed by J. D. Hirst et al. and the FEFF approach of ref [82-84]. As for NMR spectroscopy, the ^{1}H and ^{13}C chemical shielding constants were calculated from the snapshots of the CPMD/MM trajectories by employing the approach of refs [85, 86] which is based on the BLYP gradient corrected functional combined with the norm-conserving pseudopotentials of the Martins−Troullier type for the representation of the electronic structure. This approach provides very good estimations for the ^{1}H chemical shifts (the typical error with respect to the experimental values ranges from 0.5 to 1.0 ppm,[13] while for ^{13}C chemical shifts the estimations are less satisfactory but still good (the mean error is ~7.6 ppm[56]. The ^{15}N chemical shielding constants were instead computed as in ref [59], namely using ADF code[87-89] with the hybrid functional PBE0[90] and the triple-ξ singly polarized basis set TZP. This approach has been proved to provide more reliable estimations than BLYP gradient corrected functional combined with the norm-conserving pseudopotentials of the Martins−Troullier type, especially in the case of transition-metal-bounded N atoms trans to S and Cl atoms (mean error ~13-16 ppm,[59] versus ~21 ppm [56]. For the calculation of ^{195}Pt NMR shielding constants we used the ADF code[87-89] with the quadruple-ζ quadruply polarized basis set QZ4P for Pt, the triple-ζ singly polarized basis set TZP for the other QM atoms and the PBE functional.[91] This choice of basis sets and functional was shown to give reliable results for the calculation of ^{195}Pt chemical shifts.[83] For both ^{15}N and ^{195}Pt NMR chemical shifts calculations, scalar relativistic effects were taken into account with the zero-order regular approximation (ZORA) approach,[92, 93] and the MM atoms were included as point

charges. The chemical shielding constants were then converted to NMR chemical shifts relative to tetramethylsilane (TMS) in the case of ^{1}H and ^{13}C nuclei, liquid ammonia in the case of ^{15}N nuclei and Sodium hexachloroplatinate (Na_2PtCl_6) in the case of ^{195}Pt. To reduce systematic errors in calculating the chemical shifts of ^{13}C and ^{15}N nuclei, we introduced secondary references, namely C_2H_6 for ^{13}C, [94] and cisplatin, $Pt(NH_3)_2Cl_2$ in water, for ^{15}N.

3.3 Force matching.

The force matching procedure of references [23, 24] was applied to the snapshots sampled along the CPMD/MM simulations of Mets7-Pt and Pt-DNA*HMGB1A adducts. The atomic partial charges were obtained through a fit to the electrostatic potential and the electric field. These, along with van der Waals parameters taken from the used Amber force field were subtracted from the total forces acting on the QM atoms to yield the bonded forces. A least-squares fit of the latter allowed us to obtain the AMBER-type bond, angle, and dihedral angle force field parameters. Equilibrium bond lengths and bond angles were taken from the CPMD/MM averaged values.[25,26]

4. Conclusions

Hybrid CPMD/MM simulations provided the first quantitative molecular view of the 3D structures of the platinated adducts in solution involved in the pre-target resistance.[25, 27, 28] The comparison between experimental and theoretical spectroscopy data has proved the accuracy of the predicted models, as well as the robustness of the methodology in discriminating the correct binding modes from false positives (i.e. binding modes chemically plausible yet different from the one inferred from the experiments).
Hybrid CPMD/MM simulations were also successfully used to derive amber-like[18] parameters for the Pt-moieties bound to DNA[26] by using the force matching method. This is a key step in the study of the molecular recognition process between Pt-DNA and the High Mobility Group Box proteins 1A (HMGB1A). The process appears to be enthalpy driven, as found in other DNA/protein complexes,[95-97] and our calculated free energy is fairly consistent with the experimental data.[65] Our calculations also provide a structural basis for the experimentally observed decrease in affinity upon protein oxidation of HMGB1A and consequent formation of a Cys22-Cys44 disulfide bridge (5.5 kJ/mol).[65] This is consistent with the hypothesis that the high efficacy of cisplatin towards testicular tumors could be due to the exclusive presence in the testis of a member of the HMGB superfamily (the HMGB4 protein)[64, 65] that lacks one of the two cysteine residues, and therefore, cannot form the S-S bridge upon oxidation. The latter result is rather remarkable since it shows that computational methods can correctly evaluate loss of stability consequent to small conformational changes.

In conclusion, first principle simulations have shed a light on structural and energetic determinants of biomolecules involved in cisplatin-resistance. This type of approach could be extended to the very large variety of transition-metal based anticancer drugs.

Acknowledgements. The authors acknowledge the Deutsche Forschungsgemeinschaft (DFG) for financial support (Grant No. CA 973/8-1).

Bibliography

1. M. A. Fuertes, C. Alonso and J. M. Perez, Chemical reviews **103** (3), 645-662 (2003).
2. Y. Jung and S. J. Lippard, Chemical reviews **107** (5), 1387-1407 (2007).
3. L. Kelland, Nature reviews. Cancer **7** (8), 573-584 (2007).
4. M. D. Hall, M. Okabe, D. W. Shen, X. J. Liang and M. M. Gottesman, Annual review of pharmacology and toxicology **48**, 495-535 (2008).
5. B. Lippert, in *Cisplatin: Chemistry and Biochemistry of a Leading Anticancer Drug*, edited by B. Lippert (Verlag Helvetica Chimica Acta, Zürich, 2006), pp. 377-403.
6. D. Wang and S. J. Lippard, Nature reviews. Drug discovery **4** (4), 307-320 (2005).
7. V. Brabec, Progress in Nucleic Acid Research and Molecular Biology **71**, 68 (2002).
8. E. R. Jamieson and S. J. Lippard, Chem Rev **99** (9), 2467-2498 (1999).
9. L. Galluzzi, L. Senovilla, I. Vitale, J. Michels, I. Martins, O. Kepp, M. Castedo and G. Kroemer, Oncogene, 1-15 (2011).
10. F. Arnesano and G. Natile, Coordin Chem Rev **253** (15-16), 2070-2081 (2009).
11. R. Car and M. Parrinello, Phys. Rev. Lett. **55** (22), 2471-2474 (1985).
12. A. Laio, J. VandeVondele and U. Rothlisberger, J. Chem. Phys. **116** (16), 6941-6947 (2002).
13. CPMD, http://www.cpmd.org/, Copyright IBM Corp 1990-2008, Copyright MPI fu¨r Festk¨orperforschung Stuttgart 1997-2001.
14. F. Furche and J. P. J. P. Perdew, J. Chem. Phys. **124**, 044103-044127 (2006).
15. J. N. Harvey, in *PRINCIPLES AND APPLICATIONS OF DENSITY FUNCTIONAL THEORY IN INORGANIC CHEMISTRY*, edited by N. Kaltsoyannis and J. E. McGrady (Springer, 2004), Vol. 112, pp. 151-183.
16. A. J. Vlček and S. Záliš, Coordin Chem Rev **251** (3-4), 258-287 (2007).
17. Y. Zhao and D. G. Truhlar, Acc. Chem. Res. **41** (2), 157-167 (2008).
18. W. D. Cornell, P. Cieplak, C. I. Bayly, K. M. Gould, K. M. Merz, D. M. Ferguson, G. L. Seibel, U. C. Singh, P. K. Weiner and P. A. Kollmann, J. Am. Chem. Soc. **117**, 5179 (1995).
19. W. R. P. Scott, P. H. H\"unenberger, I. G. Tironi, A. E. Mark, S. R. Billeter, J. Fennen, A. E. Torda, T. Huber, P. Kr\"uger and W. F. van Gunsteren, J. Phys. Chem. A **103**, 3596 (1999).
20. A. D. MacKerell, J. J. Wiorkiewicz-Kuczera and M. Karplus, J. Am. Chem. Soc. **117**, 11946 (2000).
21. E. Ippoliti, J. Dreyer, P. Carloni and U. Rothlisberger, Lecture Notes **10**, 163–181 (2012).
22. H. M. Senn and W. Thiel, Angewandte Chemie International Edition in English **48** (7), 1198-1229 (2009).
23. P. Maurer, A. Laio, H. W. Hugosson, M. C. Colombo and U. Rothlisberger, J Chem Theory Comput **3** (2), 628-639 (2007).
24. K. Spiegel, A. Magistrato, P. Maurer, P. Ruggerone, U. Rothlisberger, P. Carloni, J. Reedijk and M. L. Klein, Journal of Computational Chemistry **29** (1), 38-49 (2008).
25. T. H. Nguyen, F. Arnesano, S. Scintilla, G. Rossetti, E. Ippoliti, P. Carloni and G. Natile, J Chem Theory Comput **8** (8), 2912-2920 (2012).
26. T. H. Nguyen, G. Rossetti, F. Arnesano, E. Ippoliti, G. Natile and P. Carloni, J Chem Theory Comput **10** (8), 3578–3584 (2014).
27. V. Calandrini, F. Arnesano, A. Galliani, T. H. Nguyen, E. Ippoliti, P. Carloni and G. Natile, Dalton Transactions **43**, 12085-12094 (2014).

28. V. Calandrini, T. H. Nguyen, F. Arnesano, A. Galliani, E. Ippoliti, P. Carloni and G. Natile, Chemistry A European Journal **20** (37), 11719–11725 (2014).
29. S. B. Howell, R. Safaei, C. A. Larson and M. J. Sailor, Molecular pharmacology **77** (6), 887-894 (2010).
30. R. Safaei, Cancer letters **234** (1), 34-39 (2006).
31. R. Safaei and S. B. Howell, Critical reviews in oncology/hematology **53** (1), 13-23 (2005).
32. T. Furukawa, M. Komatsu, R. Ikeda, K. Tsujikawa and S. Akiyama, Current Medicinal Chemistry **15** (30), 3268-3278 (2008).
33. M. T. Kuo, H. H. W. Chen, I.-S. Song, N. Savaraj and T. Ishikawa, in *Cancer and Metastasis Reviews* (Kluwer Academic Publishers-Plenum Publishers, 2007), Vol. 26, pp. 71-83.
34. S. Ishida, J. Lee, D. J. Thiele and I. Herskowitz, Proceedings of the National Academy of Sciences of the United States of America **99** (22), 14298-14302 (2002).
35. M. Komatsu, T. Sumizawa, M. Mutoh, Z. S. Chen, K. Terada, T. Furukawa, X. L. Yang, H. Gao, N. Miura, T. Sugiyama and S. Akiyama, Cancer research **60** (5), 1312-1316 (2000).
36. G. Samimi, R. Safaei, K. Katano, A. K. Holzer, M. Rochdi, M. Tomioka, M. Goodman and S. B. Howell, Clinical cancer research : an official journal of the American Association for Cancer Research **10** (14), 4661-4669 (2004).
37. N. V. Dolgova, S. Nokhrin, C. H. Yu, G. N. George and O. Y. Dmitriev, The Biochemical journal **454** (1), 147-156 (2013).
38. M. E. Palm-Espling, C. D. Andersson, E. Bjorn, A. Linusson and P. Wittung-Stafshede, PloS one **8** (7), e70473 (2013).
39. R. Safaei, M. H. Maktabi, B. G. Blair, C. A. Larson and S. B. Howell, Journal of inorganic biochemistry **103** (3), 333-341 (2009).
40. S. Itoh, H. W. Kim, O. Nakagawa, K. Ozumi, S. M. Lessner, H. Aoki, K. Akram, R. D. McKinney, M. Ushio-Fukai and T. Fukai, Journal of Biological Chemistry **283** (14), 9157-9167 (2008).
41. Z. Wu, Q. Liu, X. Liang, X. Yang, N. Wang, X. Wang, H. Sun, Y. Lu and Z. Guo, Journal of biological inorganic chemistry : JBIC : a publication of the Society of Biological Inorganic Chemistry **14** (8), 1313-1323 (2009).
42. S. E. Crider, R. J. Holbrook and K. J. Franz, Metallomics : integrated biometal science **2** (1), 74-83 (2010).
43. F. Arnesano, S. Scintilla and G. Natile, Angew. Chem., Int. Ed. **46** (47), 9062-9064 (2007).
44. Wang and Z. Guo, Anti-cancer agents in medicinal chemistry **7** (1), 19-34 (2007).
45. D. Achila, L. Banci, I. Bertini, J. Bunce, S. Ciofi-Baffoni and D. L. Huffman, Proceedings of the National Academy of Sciences of the United States of America **103** (15), 5729-5734 (2006).
46. L. Banci, I. Bertini, F. Cantini, A. C. Rosenzweig and L. A. Yatsunyk, Biochemistry **47** (28), 7423-7429 (2008).
47. O. Y. Dmitriev, Biochemistry and cell biology = Biochimie et biologie cellulaire **89** (2), 138-147 (2011).
48. N. V. Dolgova, D. Olson, S. Lutsenko and O. Y. Dmitriev, The Biochemical journal **419** (1), 51-56 (2009).
49. K. Leonhardt, R. Gebhardt, J. Mössner, S. Lutsenko and D. Huster, Journal of Biological Chemistry **284**, 7793-7802 (2009).
50. R. Safaei, P. L. Adams, M. H. Maktabi, R. A. Mathews and S. B. Howell, Journal of inorganic biochemistry **110**, 8-17 (2012).
51. T. M. DeSilva, G. Veglia and S. J. Opella, Proteins **61** (4), 1038-1049 (2005).

52. F. Arnesano, L. Banci, I. Bertini, I. C. Felli, M. Losacco and G. Natile, Journal of the American Chemical Society **133** (45), 18361-18369 (2011).
53. C. M. Sze, Z. Shi, G. N. Khairallah, L. Feketeova, R. A. O'Hair, Z. Xiao, P. S. Donnelly and A. G. Wedd, Metallomics : integrated biometal science **5** (8), 946-954 (2013).
54. A. K. Boal and A. C. Rosenzweig, Journal of the American Chemical Society **131** (40), 14196-14197 (2009).
55. P. Liu, B. Kim, R. A. Friesner and B. J. Berne, Proc Natl Acad Sci U S A. **102** (39), 13749-13754 (2005).
56. J. R. Cheeseman, G. W. Trucks, T. A. Keith and M. J. Frisch, Journal of Chemical Physics **104** (14), 5497-5509 (1996).
57. T. G. Appleton, J. W. Connor, J. R. Hall and P. D. Prenzler, Inorganic Chemistry **28** (11), 2030-2037 (1989).
58. T. G. Appleton, J. R. Hall and S. F. Ralph, Inorganic Chemistry **24** (26), 4685-4693 (1985).
59. J. Vicha, M. Patzschke and R. Marek, Physical Chemistry Chemical Physics **15**, 7740-7754 (2013).
60. I. Ugrinova, S. Zlateva, I. G. Pashev and E. A. Pasheva, Int J Biochem Cell Biol **41** (7), 1556-1562 (2009).
61. J. C. Huang, D. B. Zamble, J. T. Reardon, S. J. Lippard and A. Sancar, Proc. Natl. Acad. Sci. U S A **91** (22), 10394-10398 (1994).
62. J. Malina, J. Kasparkova, G. Natile and V. Brabec, Chemistry & biology **9** (5), 629-638 (2002).
63. S. Yusein-Myashkova, I. Ugrinova and E. Pasheva, BMB reports (2013).
64. R. Catena, E. Escoffier, C. Caron, S. Khochbin, I. Martianov and I. Davidson, Biology of reproduction **80** (2), 358-366 (2009).
65. S. Park and S. J. Lippard, Biochemistry **50** (13), 2567-2574 (2011).
66. U. M. Ohndorf, M. A. Rould, Q. He, C. O. Pabo and S. J. Lippard, Nature **399** (6737), 708-712 (1999).
67. A. Barducci, G. Bussi and M. Parrinello, Phys Rev Lett **100** (2), 020603 (2008).
68. A. Laio and M. Parrinello, Proc. Natl. Acad. Sci. U S A **99** (20), 12562-12566 (2002).
69. P. Raiteri, A. Laio, F. L. Gervasio, C. Micheletti and M. Parrinello, J. Phys. Chem. B **110** (8), 3533-3539 (2006).
70. V. Leone, F. Marinelli, P. Carloni and M. Parrinello, Curr. Opin. Struct. Biol. **20** (2), 148-154 (2010).
71. A. D. Becke, Physical Review A **38** (6), 3098-3100 (1988).
72. C. Lee, W. Yang and R. G. Parr, Phys. Rev. B **37** (2), 785-789 (1988).
73. N. Troullier and J. L. Martins, Phys. Rev. B **43** (3), 1993-2006 (1991).
74. O. A. von Lilienfeld, I. Tavernelli, U. Rothlisberger and D. Sebastiani, Journal of Chemical Physics **122** (1), 014113-014118 (2005).
75. G. J. Martyna and M. E. Tuckerman, Journal of Chemical Physics **110** (6), 2810-2821 (1999).
76. J. Wang, P. Cieplak and P. A. Kollman, Journal of Computational Chemistry **21** (12), 1049-1074 (2000).
77. V. Hornak, R. Abel, A. Okur, B. Strockbine, A. Roitberg and C. Simmerling, Proteins: Structure, Function, and Bioinformatics **65** (3), 712-725 (2006).
78. K. Lindorff-Larsen, S. Piana, K. Palmo, P. Maragakis, J. L. Klepeis, R. O. Dror and D. E. Shaw, Proteins **78** (8), 1950-1958 (2010).
79. W. L. Jorgensen, J. Chandrasekhar, J. D. Madura, R. W. Impey and M. L. Klein, Journal of Chemical Physics **79** (2), 926-935 (1983).
80. D. E. Smith and L. X. Dang, Journal of Chemical Physics **100** (5), 3757-3766 (1994).
81. I. S. Joung and T. E. Cheatham, 3rd, J phys chem B **112** (30), 9020-9041 (2008).

82. J. J. Rehr, J. Mustre de Leon, S. I. Zabinsky and R. C. Albers, Journal of the American Chemical Society **113** (14), 5135-5140 (1991).
83. J. J. Rehr, R. C. Albers and S. I. Zabinsky, Physical Review Letters **69** (23), 3397-3400 (1992).
84. J. J. Rehr and R. C. Albers, Reviews of Modern Physics **72** (3), 621-654 (2000).
85. A. Putrino, D. Sebastiani and M. Parrinello, Journal of Chemical Physics **113** (17), 7102-7109 (2000).
86. D. Sebastiani and M. Parrinello, J. Phys. Chem. A **105** (10), 1951-1958 (2001).
87. G. te Velde, F. M. Bickelhaupt, E. J. Baerends, C. Fonseca Guerra, S. J. A. van Gisbergen, J. G. Snijders and T. Ziegler, Journal of Computational Chemistry **22** (9), 931-967 (2001).
88. C. Fonseca Guerra, J. G. Snijders, G. te Velde and E. J. Baerends, Theor Chem Acc **99** (6), 391-403 (1998).
89. ADF2013, in *Scientific Computing & Modelling NV*, edited by T. C. Vrije Universiteit (De Boelelaan 1083; 1081 HV Amsterdam; The Netherlands).
90. C. Adamo and V. Barone, Journal of Chemical Physics **110**, 6158-6169 (1999).
91. B. Hammer, L. B. Hansen and J. K. Nørskov, Physical Review B **59** (11), 7413-7421 (1999).
92. E. van Lenthe, A. Ehlers and E.-J. Baerends, Journal of Chemical Physics **110**, 8943-8953 (1999).
93. E. van Lenthe, J. G. Snijders and E. J. Baerends, Journal of Chemical Physics **105**, 6505-6516 (1996).
94. U. F. Röhrig and D. Sebastiani, J. Phys. Chem. B **112** (4), 1267-1274 (2008).
95. S. Joynt, V. Morillo and F. Leng, Biophysical journal **96** (10), 4144-4152 (2009).
96. E. Vaz de Andrade, S. M. Freitas, M. M. Ventura, A. Q. Maranhao and M. M. Brigido, Biochimica et biophysica acta **1726** (3), 293-301 (2005).
97. T. Cui, S. Wei, K. Brew and F. Leng, Journal of molecular biology **352** (3), 629-645 (2005).